Journal of Atmospheric and Solar-Terrestrial Physics 179 (2018) 517–526

Contents lists available at ScienceDirect

Journal of Atmospheric and Solar-Terrestrial Physics

journal homepage: www.elsevier.com/locate/jastp

# Comparative analysis of the proton generation efficiency during 17 March 2003 and 11 April 2004 solar flares

A.V. Bogomolov[a,*], I.N. Myagkova[a], I. Myshyakov[b], Ts Tsvetkov[c], L. Kashapova[b], R. Miteva[d]

[a] Skobeltsyn Institute of Nuclear Physics, MSU, Moscow, Russia
[b] Institute of Solar-Terrestrial Physics SB RAS, Irkutsk, Russia
[c] Institute of Astronomy and National Astronomical Observatory, Bulgarian Academy of Sciences, Sofia, Bulgaria
[d] Space Research and Technology Institute, Bulgarian Academy of Sciences, Sofia, Bulgaria

ARTICLE INFO

*Keywords:*
Solar energetic particles
Solar flare
Flare emission signatures

ABSTRACT

We present the comparative analysis of the solar energetic particle (SEP) event properties and the indicators of acceleration processes in solar flares – the hard X-rays (HXR) and radio emission from microwaves to the meter-range. We focus our study on the two SEP events associated with solar flares with similar characteristics in HXR emission and the close location on solar disk. The proton flux in the SEP event associated with the weaker flare by GOES class in soft X-ray (SXR) (C9.6/SOL2004-Apr-11) was more than an order higher than in the SEP event associated with the more powerful solar flare (X1.5/SOL2003-Mar-17). At the same time, the electron fluxes in both SEP events were comparable. Both flares were followed by CMEs with speed above 1000 km $s^{-1}$. The analysis of SEP fluxes and flare plasma parameters was done taking into account the magnetic topology of the active region (AR) and its evolution before and during the solar flares. The 3D reconstruction of the potential magnetic field showed the existence of an arcade of high loops covering the active region where the more powerful flare occurred. The flare associated with the proton-rich SEP event occurred in the active region where 3D reconstruction revealed a fan of high loops associated with open magnetic field lines. We suppose that the arcade of high loops could be the factor which prevents an escape of the accelerated particles into the interplanetary space (IPS) while the fan of high loops facilitates the production of the more proton-rich SEP events. Results of the analysis show a necessity to use topology of ARs as a parameter in statistical studies of SEP event origins.

## 1. Introduction

Solar energetic particles (SEPs) are the observed in situ electrons, protons and heavy nuclei at energies from the keV up to the GeV range (Klecker et al., 2006; Desai and Giacalone, 2016). The need for improved physical understanding on the acceleration, escape and transport processes from the solar source to the given particle detector has been long recognized, see recent summary by Klein and Dalla (2017). SEPs, together with the effects caused by their solar origin, flares and coronal mass ejections (CMEs) (Klein and Trottet, 2001; Bazilevskaya, 2017) are important space weather agents and topic of focused research. Filaments have also been proposed in relation to in situ particle increases (Kahler et al., 1986; Gopalswamy et al., 2015) based on selected case studies. Despite that the key principles of particle acceleration that takes place in solar flares, and CMEs are long been known (Vainio and Afanasief, 2018), there is still some ambiguity about the time and place of the particle escape from the acceleration site as well as the exact travel path through the interplanetary space in deviation from the standard Parker spiral. Such uncertainty results due to the lack of direct (in situ) particle observations on route.

While in space, humans and technological devices are exposed to different radiation effects caused by energetic particles – namely ones of solar origin (Jiggens et al., 2014), galactic cosmic rays (GCR) (Semkova et al., 2018) and particles of the radiation belt of the Earth (Iucci et al., 2005). Based on the available experimental data variations of the non-solar origin protons with energies of ten to hundreds MeV (the protons of the inner radiation belt of the Earth and galactic cosmic rays) are small in comparison with fluxes of protons in SEP events. Thus we can neglect their contribution.

Such risks serve as an additional motivation to build reliable forecasts for the particle occurrence, time of arrival and properties. Physical and empirical models use as input a set of observables related to their probable solar origin. For example, present-day SEP alerts which are built on real-time data use exclusively solar flare information (e.g., flux

* Corresponding author.
*E-mail address:* aabboogg@sinp.msu.ru (A.V. Bogomolov).

https://doi.org/10.1016/j.jastp.2018.08.010
Received 14 March 2018; Received in revised form 8 August 2018; Accepted 14 August 2018
Available online 22 August 2018

and location by Núñez (2011)) due to their availability. Statistical results based on large sample of historical data (Cane et al., 2010; Miteva et al., 2018), however, show there is a large scatter while building relationships between particles and flares/CMEs and a dominant accelerator is not possible to identify within the uncertainty of the analysis. In addition, the same particle flux can be associated to flares and CMEs with properties that cover a wide range in terms of their class and speed, respectively. Complementary, detailed case studies are needed in order to identify and weight the importance of the different reasons for such observational fact. Among the probable causes to be considered are the effects of prolonged acceleration process, coronal trapping vs. ready escape route for the particles, preferential magnetic connection established to the spacecraft. Magnetic field line extrapolations offer a tool to visualize the large scale magnetic field line configuration in the solar corona that is not always illuminated by hot plasma flows. Finally, a set of different models aim to bridge the gap between the remote observation of phenomena close to the Sun and the near-Earth structures reconstructed based on in situ data obtained at 1 AU, e.g. particle propagation models (Klein and Dalla, 2017) and CME propagation models (e.g. Zhao et al., 2016).

The current study presents a comparative analysis of all solar flares with hard X-rays (HXR) emission observed with high temporal resolution by SOlar Neutrons and Gammas (SONG) instrument in the experiment on board *Complex Orbital Near-Earth Observations of Solar Activity* (CORONAS-F) satellite (Kuznetsov et al., 2014) that are associated with SEP events based on data obtained by *Advanced Composition Explorer* (ACE) spacecraft (see details below) and *Geostationary Operational Environmental Satellite* (GOES). The target of this analysis is to reveal that both, powerful and weak, SEP events are associated with solar flares observed by SONG instrument. Since we are interested also in the location of the HXR source, flare data provided by the *The Reuven Ramaty High Energy Solar Spectroscopic Imager* (RHESSI) (Lin et al., 2002) is also included in the analysis. We selected several events after applying the above criteria. Among the event candidates, there were two cases with a strong response in HXR emission but related with significantly different proton fluxes.

As HXR emission is the result of the participation of accelerated electrons then nowadays it is the most commonly used indicator of electron acceleration in a solar flare. We do not observe the direct markers of proton acceleration as frequently as in the case of electrons. There are direct observations of X-ray emission with energies above 800 keV and γ-ray emission. The results indicate that proton acceleration usually occurs during the main flare phase but not simultaneously with rising of HXR emission generated by electrons (see, for example, Grechnev et al., 2008). However, these processes take place in the same magnetic field structures and they are undoubtedly closely related. In addition to acceleration during the impulse phase of the flares, we have evidence of the acceleration processes during the gradual phase of solar flares that may contribute to SEP fluxes (Chertok, 1995; Akimov et al., 1996; Klein and Trottet, 2001; Zimovets and Struminsky, 2012). There are so-called the Long Duration Events (LDE) which gradual phases may continue for several hours. Thus, the duration of comparable events should be less the at least a couple hours. Thus, the reason for selection of these two events is the similar initial particle acceleration causing SEP events with different characteristics. The aim of our study is to use a comparative analysis of the parameters of the flares, ARs and SEP events for investigating the possible reasons that resulted in SEP events.

## 2. Observations and data analysis: comparison of the event characteristics

For the present study two events are selected. The first event is the X1.5 GOES class flare[1] that occurred on March 17, 2003 (the SOL2003-Mar-17 event). The onset is at about 18:55 UT and maximum at about 19:04 UT. The flare took place in an AR 10314 in the south-western part of solar disk (X = 580, Y = − 150 arc seconds or S14W39). We related this solar flare with a CME which according to the LASCO catalogue (Gopalswamy et al., 2009)[2] has linear speed 1020 km s$^{-1}$, f angular width (AW) of 96° and measurement position angle (MPA) of 264° (the CME was directed westwards). The second event is a C9.6 GOES class flare that occurred on April 11, 2004 (the SOL2004-Apr-11 event) in AR 10588 (X = 670, Y = − 200 arc seconds or S16W46). From the coordinates of ARs, one can see that the position of AR 10314 and AR 10588 on solar disk during the analyzed events was nearly the same. The onset and maximum is reported at about 03:57 UT and at about 04:18 UT, respectively. It was associated with the CME with linear speed of 1645 km s$^{-1}$, AW is 314° and MPA is 237° (directed south-west). The characteristics of both events are analyzed and compared using observations of solar flare emission in X-rays, extreme ultraviolet (EUV) and the radio range, line-of-sight (LOS) magnetograms and in the libration point L1 SEP observations.

### 2.1. SEP parameters

Information about the solar proton and electron fluxes observed during the considered SEP events is taken from the measurements carried out on board *Advanced Composition Explorer (ACE spacecraft*, located in the libration point L1 at about 1.5 million km from the Earth to the Sun (Stone et al., 1998). It measures high energy proton flux in two energy channels, namely >10 MeV and >30 MeV integrated proton flux (*Solar Isotope Spectrometer* (SIS) instrument). The electron fluxes in four energy channels from 38 keV up to 315 keV were measured by *Electron, Proton, and Alpha Monitor* (EPAM) instrument also on board *ACE spacecraft*. We used two energy channels, 38−53 keV and 175−315 keV. The decision to prefer data from the spacecraft was due to the fact that it is located outside the Earth's magnetosphere.

Fig. 1 shows the time profiles of proton and electron fluxes over the selected time period. The information about the flux maxima and fluences of electrons and protons obtained after subtraction of the background is presented in Table 1. During the SOL2004-Apr-11 event, the maximal flux of solar protons with an energy > 30 MeV reached its peak value about 3 h earlier than the flux of 10-MeV protons. During the SOL2003-Mar-17 the maxima of solar proton flux with energy more than 10 MeV and more than 30 MeV were observed simultaneously. One can see that the proton flux in SOL2004-Apr-11 event is stronger in comparison to the event in SOL2003-Mar-17. We obtained consistent results based on data from a different spacecraft, *Energetic and Relativistic Nuclei and Electron* (ERNE) experiment (Torsti et al., 1995) aboard SOHO mission. We note that the spectrum of the proton flux in the SOL2004-Apr-11 SEP event was significantly softer than during the SOL2003-Mar-17 event. The ratio of the maximal fluxes in the channels > 10/> 30 MeV is 17.4 during the SOL2004-Apr-11 event, while the ratio is 6 for the SOL2003-Mar-17 event. The ratios of the proton fluences in the channels > 10/> 30 MeV are 12.3 and 7.3, respectively. For the SEP protons, the ratio of the flux maximum in SOL2004-Apr-11 event to the similar parameter in SOL2003-Mar-17 event is 18 for the protons with energy above 30 MeV and about 50 for the protons with energies above 10 MeV. The ratios of the fluences in the same channels are 86 and 145, respectively.

We see a slightly different situation for the flux of the SEP electrons (see, Fig. 1 and Table 1). The maximal flux of SEP electrons in the 175 − 315 keV channel during the SOL2004-Apr-11 event was about three times higher according to ACE data relative to the SOL2003-Mar-17 event. Moreover the maximum flux of the low-energy SEP electrons (38 − 53 keV channel) during the SOL2003-Mar-17 event even slightly exceeds the maximum flux during the SOL2004-Apr-11 event.

Thus, the ratio of the maximum proton and electron fluxes in the

[1] http://www.swpc.noaa.gov/.

[2] https://cdaw.gsfc.nasa.gov/CME_list/.

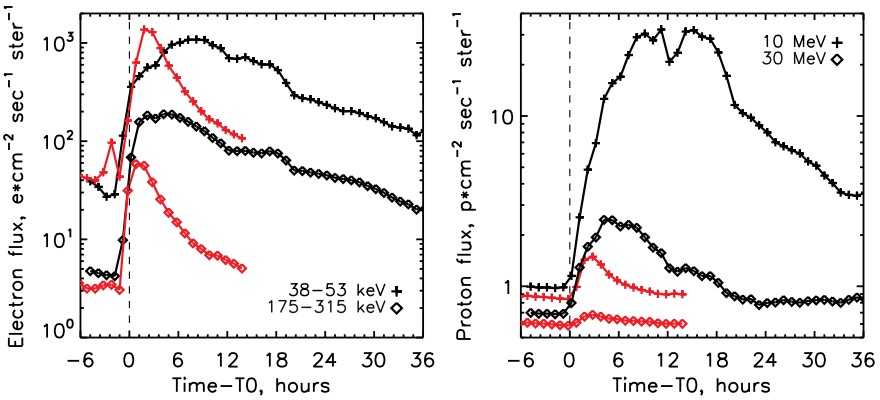


**Fig. 1.** Temporal evolution of the proton and electron fluxes during the events in March 2003 (red color) and April 2004 (black color). The left panel shows an evolution of the SEP electron fluxes and the right panel shows the SEP proton fluxes. The time profiles of both events are plotted relative to zero time. The zero time is 19:12 UT for the SOL2003-Mar-17 event and 04:48 UT for the SOL2004-Apr-11 event. (For interpretation of the references to color in this figure legend, the reader is referred to the Web version of this article.)

**Table 1**
The parameters of electron and proton fluxes in the SEP events. The maxima of the fluxes are particles/($cm^2$ *sr s*) and the fluences are particles/($cm^2$ *sr*).

| | SOL2013-Mar-17 | SOL2014Apr-11 |
|---|---|---|
| Maximum of $F_e$, $E$ = 38 − 53 keV | 1330 | 1070 |
| $F_e$ fluence, $E$ = 38 − 53 keV | $2.3 \times 10^7$ | $6.4 \times 10^7$ |
| Maximum of $F_e$, $E$ = 175 − 315 keV | 56 | 190 |
| $F_e$ fluence, $E$ = 175 − 315 keV | $9.4 \times 10^5$ | $1.1 \times 10^7$ |
| Maximum of $F_p$, $E$>10 MeV | 0.6 | 31.3 |
| $F_p$ fluence, $E$> 10 MeV | $1.1 \times 10^4$ | $1.6 \times 10^6$ |
| Maximum of $F_p$, $E$>30 MeV | 0.1 | 1.8 |
| $F_p$ fluence, $E$>30 MeV | $1.5 \times 10^3$ | $1.3 \times 10^5$ |

highest-energy channels measured on board ACE spacecraft is $1.8 \times 10^{-3}$ for the March 2003 event and $10^{-2}$ for the April 2004 one (ratios of proton and electron fluences are $1.6 \times 10^{-3}$ and $1.2 \times 10^{-2}$, respectively). If we compare the SEP proton productivity of the analyzed events, then it turns out the less powerful according to GOES classification flare (C9.6, SOL2004-Apr-11) produced about one order of magnitude higher proton flux (according to fluences) than the more powerful X1.5 flare (SOL2003-Mar-17).

### 2.2. X-rays and radio time profiles, spectral indexes from MW and X-ray

We analyzed the evolution of the different processes based on the time profiles of X-ray and radio emission. Flare plasma heating is traditionally studied using the soft X-ray (SXR) flux observed by GOES. We choose the 1 − 8 Å band because it is equivalent to 1.5 − 12 keV energy band and better tracks the thermal processes.

The response of the non-thermal processes in X-ray emission is analyzed in two ways. The direct way assumes analysis of the X-ray data in energy band 60 − 150 keV that is surely formed by accelerated electrons. Our analysis is based on the hard X-ray data from solar flares obtained by the SONG (SOlar Neutrons and Gamma-rays) multichannel gamma-ray spectrometer which operated onboard CORONAS-F solar space low-altitude observatory from the middle of 2001 until the end of 2005 (Kuznetsov et al., 2006, 2014). The hard X-ray and γ-ray radiation were detected by the SONG instrument with the time resolution of the device was 2 − 4 s in the energy range 30 keV − 300 MeV. The detailed description of the SONG instrument and the data processing technique is described in (Kuznetsov et al., 2014; Bogomolov et al., 2014). During the running time of the SONG, the energy threshold values increased by $k$ times relative to the beginning of experiment because of changing the detector properties. In March 2003 (SOL2003-Mar-17 event) the coefficient $k$ was equal to 1.25 and in April 2004 (SOL2004-Apr-11) − to 1.45.

The lowest energy threshold provided by SONG was about 40 keV. It means that we could be sure that the using HXR time profiles demonstrate the evolution of accelerated electrons. However, there are electrons with energies above 18 − 20 keV but lower 40 keV in X-ray photon spectrum. They usually belong to the population of the accelerated electrons and carry information about energy release processes. We used the time derivative of the soft X-ray GOES emission to trace this kind of electrons. This technique is based on the Neupert effect (Neupert, 1968; Dennis and Zarro, 1993). This effect shows evolution of the electrons which produce thermal X-ray emission and often this derivative coincides with non-thermal X-ray emission with energies at about 20–30 keV. We used the time profile of this parameter for comparison with the time profiles of the other spectral bands shown in Fig. 2. As we can see in Fig. 2 the duration of the SXR time derivative in the second flare (nearly 20 min) is nearly twice as long compared to the first event, despite the fact that the 2003-event was of much larger SXR flux.

An alternative marker of non-thermal processes is the microwave (MW) incoherent emission of accelerated electrons that is presented in our analysis by the 15.4 GHz frequency flux. We used data obtained by the Radio Solar Telescope Network (RSTN) for investigating the behavior of the temporal profiles radio emission. Single frequency radio records (in eight discrete frequencies from 245 MHz to 15.4 GHz) covering heights from low corona to upper chromosphere are available for the two events under study. We use the flux at 245 MHz for testing of the processes related with the coherent radio emission indicating to the propagation of the accelerated electrons (the type II and type III radio bursts). The comparison of time profiles of incoherent and coherent radio emission are presented in Fig. 2, panels b and d.

The stronger event in SXRs (in 2003) produces also a stronger radio flux at the various radio frequencies. The signatures in the 2004-event, however, show an increase first at low frequencies progressing to higher ones, whereas the radio emission during the 2003-event occurred nearly simultaneously at all frequencies. The presence of low-frequency type III bursts is the indicator of open field lines extend from within 0.5 solar radius into the interplanetary space (Cane et al., 2002). The resulted plots comparing the different type of emission for both events are presented on Fig. 2.

We note that both events do not show any delay of HXR emission relative to MW emission (see Fig. 2, panel b). It means that these emissions were generated by the same population of the electrons and

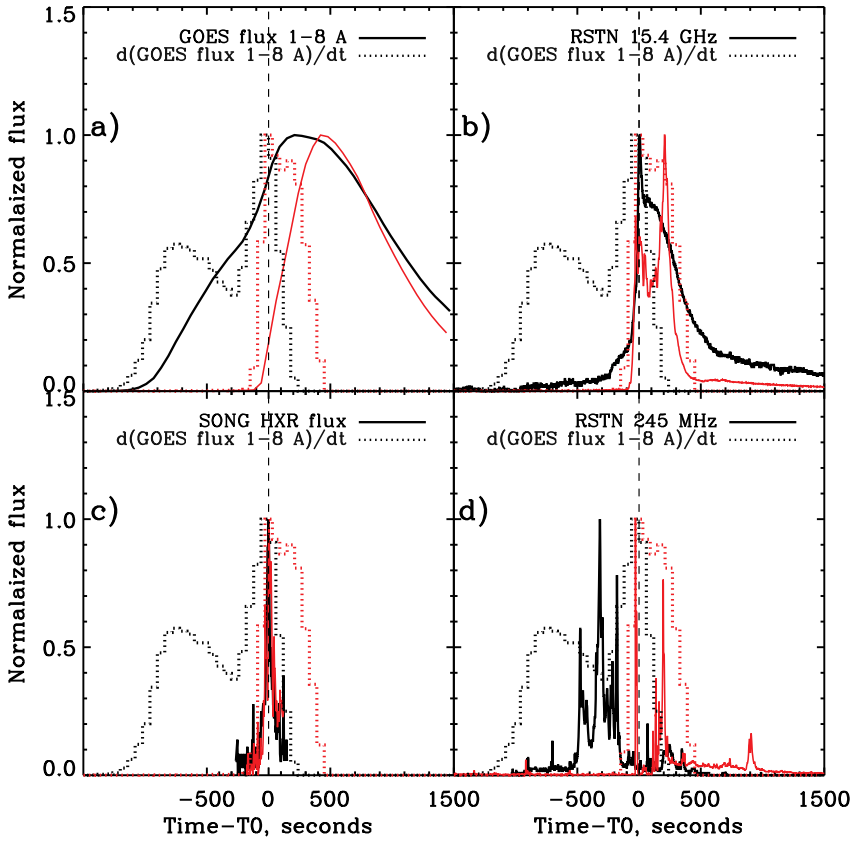


**Fig. 2.** Comparison of the time profiles in the different spectral ranges (denoted with solid lines) and the time derivative of SXR flux by GOES (denoted by d (GOES flux 1 − 8 Å)/dt with dotted lines): a) 1 − 8 Å soft X-rays by GOES; b) the microwave flux at 15.5 GHz frequency; c) hard X-ray flux by SONG (the duration of this time profile has defined by the SONG observational record length); d) radio flux at 245 MHz. The time profiles of both events are plotted relative to zero time chosen at the maximum of the hard X-ray flux of each event. It is 18:57:59 UT for the SOL2003-Mar-17 event (the red lines) and 04:15:31 UT for the SOL2004-Apr-11 event (black lines). All profiles were normalized to the maximum value. (For interpretation of the references to color in this figure legend, the reader is referred to the Web version of this article.)

we are able to compare parameters obtained from the HXR and MW. The relationship between the HXR and MW emissions in the SOL2004-Apr-11 event demonstrates the "magnetic trap effect" when MW emission decreases slower than the HXR emission. However, the trap effect is not seen during the first peak of the SOL2003-Mar-17 event. According to the derivative of SXR emission, the second peak also did not show any trapping and decreased nearly simultaneously with MW 15.4 GHz time profile.

During the SOL2004-Apr-11 event the first peak of time profiles of the SXR derivative is seen at early phase of the flares. It had neither response in HXR nor in MW emissions. Then we can see the peaks of the 245 MHz flux occurred between the first peak of the time profiles of the SXR derivative and the HXR peak marking the main phase of the flare. These behaviours could mean that at early phase of the flare small amount of the electrons with energies about 12–25 keV were generated and they did not reached the lower layers for HXR emission generation nor their energy was enough for generation of MW emission. But these generated electrons could easily escape the solar atmosphere via the open magnetic field lines that were close to the location of energy release.

The SXR flux derivative obtained for SOL2003-Mar-17 event shows agreement with the HXR peak time profile by SONG. The second peak of this time profile coincides with the second peak seen in MW emission. We note that the SONG data absence during the second peak of the SOL2003-Mar-17 event (after 19:00 UT) was caused by the CORONAS-F satellite passing through the outer radiation belt of the Earth. It resulted to high and unstable background level produced by the bremsstrahlung of the radiation belt electrons that did not permit to determine the

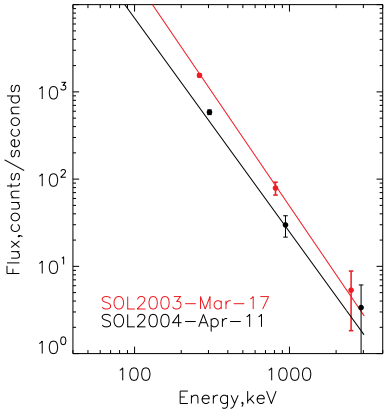


**Fig. 3.** The HXR spectra for the main peaks of the events according to the SONG data.

contribution of solar flare emission from the HXR total flux. The peaks of the time profile of the 245 MHz (coherent) emission occurred at the same time as peaks of MW and SXR derivative. However, there is no peak to peak correspondence as the emissions had different mechanism of generation.

We used SONG data for estimation of the HXR photon spectral indices γ at the main peak of the HXR time profile for each flare (Fig. 3). The photon spectral index of the power-law spectra for the March 2003 flare was estimated based on the response in channels 37.5 − 75, 75 −

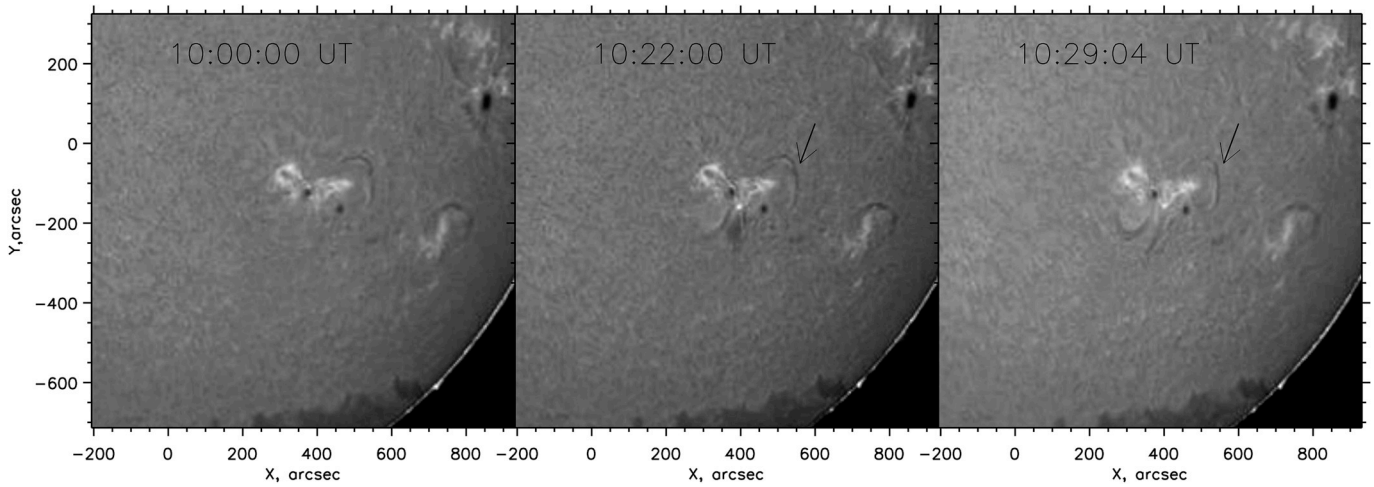


**Fig. 4.** Kanzelhöhe $H_\alpha$ observations showing evolution of AR 10314 before the event under consideration. The filament like structures are marked by arrows.

187.5, and 187.5 – 625 keV. The spectral index γ for the flare in April 2004 was calculated using 43.5 – 87, 87 – 217.5 and 217.5 – 725 keV bands. The non-thermal part of X-ray spectrum was fitted by a power law function using the least square method. We found that the spectral photon index of HXR flare emission is close to 2.6 for the event on March 17, 2003 and this parameter was about 2.5 for the event April 11, 2004. We can see in Fig. 3 that the slope of both spectra was nearly parallel to each other. At the same time, the flux of SOL2003-Mar-17 event was a slightly higher than during the other event.

### 2.3. Associated filaments according to EUV and $H_\alpha$ data

The period of observations allows us to use only data obtained by the Extreme ultraviolet Imaging Telescope (EIT).[3] This is an instrument onboard the SOHO spacecraft that obtains high-resolution images of the solar corona in the ultraviolet range. The EIT instrument observes four different spectral bands: Fe XI/X 171, Fe XII 195, Fe XV 284, and HeII 304 Å. In this paper we use 195 and 304 Å images to illustrate the filament eruptions (FEs). More detailed information is presented by (Moses et al., 1997).

The structure and behavior of the filaments before and during the flares is the important factor of an event scenario. We had the well-developed active regions with filaments for both cases. To follow the filaments in the active regions where the considering events occurred, we used $H_\alpha$ data from the solar telescope in the Kanzelhöhe Observatory for Solar and Environmental Research[4] affiliated with the Institute of Geophysics, Astrophysics and Meteorology out of the University of Graz. This observatory is part of Global high-resolution $H_\alpha$ (656.3 nm) network.[5] Also part of Global high-resolution $H_\alpha$ (656.3 nm) network is Yunnan Astronomical Observatory (YNAO).[6]

We also used data provided by RHESSI (Lin et al., 2002) for the localization of the HXR emission produced during these solar flares. Since RHESSI did not observe the main phase of the SOL2003-Mar-17 event, the 6 – 12 keV energy band image was produced only at the early onset of the flare. The images of the flare sources for the SOL2004-Apr-11 event was obtained at the maximum of the HXR emission for the 6 – 12 keV and 25 – 50 keV energy bands. The images were reconstructed with the CLEAN algorithm within the RHESSI software (Schwartz et al., 2002).

#### 2.3.1. 2003 March 17

No $H_\alpha$ observations were found during this event. We were able to analyse the morning observations obtained in Kanzelhöhe observatory. We can notice the appearance of prominence-like structure between 10:09 – 10:53 UT. It is located above the AR with legs anchored in the photosphere (Fig. 4). At 10:22 UT the legs start distancing (Fig. 4 middle) and 7 min later the material forming the legs rises up and falls back down to the Sun with arch-like motions (Fig. 4 right). At about 10:42 UT the prominence disappears after a failed eruption. The last valuable observations were obtained at 12:52 UT. The filament located north-eastern from the sunspots remains quiescent till this time without showing any signs for upcoming eruptions.

SOHO/EIT 195 Å data provides high-cadence observations of the Sun and allows us to follow the behavior of the active area (including the filament and the solar flare). About 18 h before the onset of the solar flare we can track plasma motions in the loops above the AR 10314. An eruption begins minutes after 16:30 UT, reaching the maximum signal due to solar flare in 19:16 UT. The type III radio burst is reported[7] during 18:57 – 18:59 UT, but there is no information about the type II radio burst.

We were able to reconstruct the position of the HXR flare source only for initial stage of the flare. As one can see on Fig. 5 the 12 – 25 keV flare source is located above the developing flare loop arcade (see the left panel). On the right panel we increased the brightness of the flare kernel in order to reveal the nearby filament. There is a small filament structure at north-west of the signatures of the filament eruption or evolution.

#### 2.3.2. 2004 April 11

The AR 10588 associated with the event on 2004 April 11 appeared on the eastern solar limb on April 2 without filament signatures in $H_\alpha$. Due to gaps in $H_\alpha$ data the first detection of the filament was on April 8 when the filament together with the AR passes through the central meridian. At this date, minutes after 09:00 UT an eruption of the filament was reported (observations by Kanzelhöhe observatory). The $H_\alpha$ line image by the YNAO (China) obtained on April 11 shows that the system of filaments was visible before the onset of the SOL2004-Apr-11 flare (Fig. 6). Video with the $H_\alpha$ observations from 02:12 to 05:26 is available online.[8]

[3] https://umbra.nascom.nasa.gov/eit/.
[4] https://www.kso.ac.at/index_en.php.
[5] http://www.bbso.njit.edu/Research/Halpha/ha_inst.html.
[6] http://english.ynao.cas.cn/.
[7] ftp://ftp.ngdc.noaa.gov/STP/swpc_products/daily_reports/solar_event_reports/.
[8] http://ftp.bbso.njit.edu/pub/archive/2004/04/11/ynao_halph_fi_20040411.mpg.

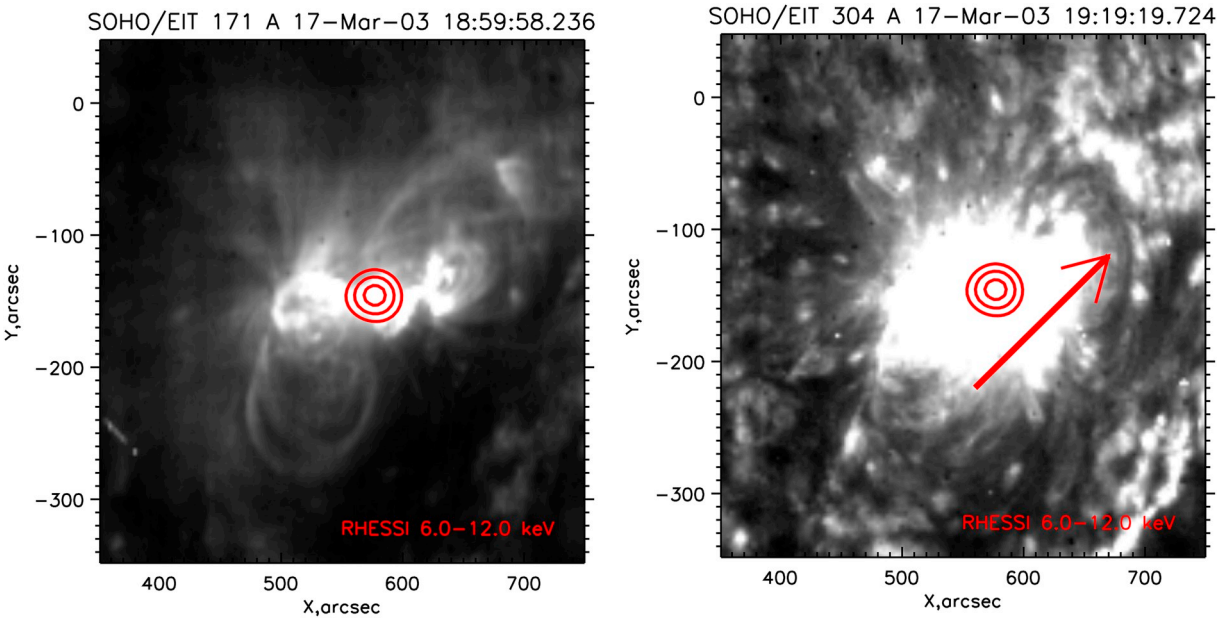


**Fig. 5.** The location of the SOL2003-Mar-17 flare in the AR. SOHO/EIT images obtained during the flare overlaid by 12 − 25 keV images obtained by RHESSI at 18:55:00 − 18:55:30 UT. Left panel: SOHO/EIT 171 Å image at 18:59:58 UT. Right panel: SOHO/EIT 304 Å image at 19:19:20 UT. The contours of X-ray sources are 50, 70 and 90% of the maximum intensity of the image. On the right panel the brightness of the flare kernel was artificially increased in order to show the nearby filament.

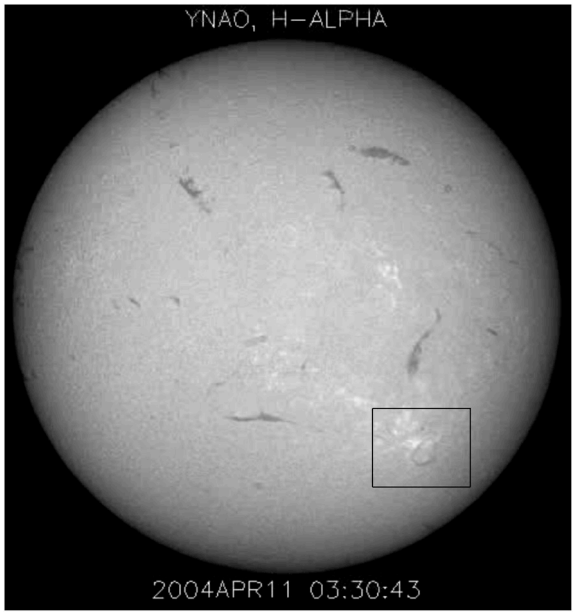


**Fig. 6.** YNAO $H_\alpha$ observations before filament eruption in SOL2004-Apr-11 event. The AR 10588 and the filament are in the south-western part of the solar disk and marked by the rectangle.

SOHO/EIT data shows the eruption from its onset. Plasma motions started after 03:00 UT and warned about the upcoming eruption that started at about 03:12 UT and lasted ~ 4 h. The early phase of the flare is shown on Fig. 7 (left panel). One can see that the southern footpoint of the filament like structure is connected with 12 − 25 keV X-ray source. This X-ray source temporarily coincided with the first peak of SXR flux derivative seen on the bottom of Fig. 2 and it is a signature of the onset of an energy release process in the flare. The image on the right panel of Fig. 7 shows the difference 195 Å image at the moment of the eruption. The dark structures correspond to a filament eruption and one can see the close connection of X-ray flare sources with it. The type III radio burst were also observed during this event[9] but in this case, they preceded the flare onset. A type II radio burst can be seen below 14 MHz[10] but is not reported at higher frequencies.

### 2.4. 3D magnetic structure nearby the flare location

Magnetic field of the considered ARs was reconstructed using Fast

[9] ftp://ftp.ngdc.noaa.gov/STP/space-weather/solar-data/solar-features/solar-radio/radio-bursts/reports/spectral-listings/.

[10] https://solar-radio.gsfc.nasa.gov/wind/data_products.html.

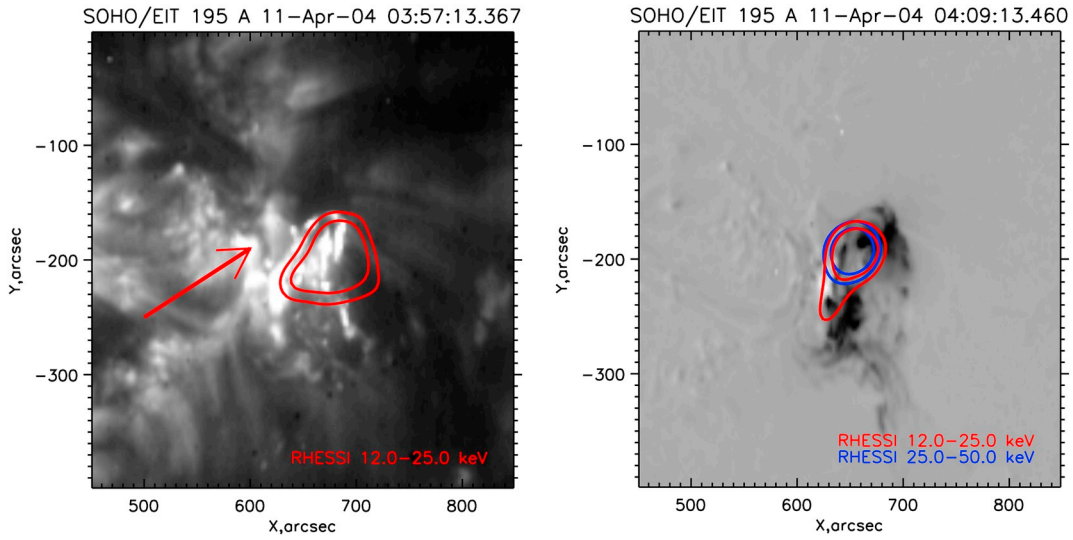


**Fig. 7.** The location of the SOL2004-Apr-11 event flare in the AR. The left panel: SOHO/EIT 195 A image at 03:57:13 UT overlaid by the 12 − 25 keV X-ray source by RHESSI within 03:59:08–04:01:16 UT. The right panel: The difference between SOHO/EIT 195 Å image at 04:09:13 UT and 03:57:13 UT. The black color shows the negative processes (like filament eruption) and the white color corresponds to the emission processes. The image overlaid by the 12 − 25 keV and 25 − 50 KeV X-ray source by RHESSI within 04:14:30 − 04:15:30 UT. The contours of X-ray sources are 30 and 50% of the maximum intensity of the image.

Fourier Transformations (FFT) based potential extrapolation. Because potential magnetic field is current-free by definition, this approach in general can not reproduce low lying nonpotential flaring loops, associated with considerable electric currents. On the other hand, potential extrapolation provides an insight on large-scale magnetic structure that remains more stable for extended periods of time. The 96-min cadence full disk line-of-sight magnetograms taken by Michelson Doppler Imager (MDI) onboard SOHO space observatory (Scherrer et al., 1995) were implemented as input data for the extrapolation. In order to obtain classical Neumann boundary conditions, normal magnetic field component was derived from initial line-of-sight magnetograms, assuming that photosphere magnetic field is radial (Wang and Sheeley, 1992):

$$\mathbf{B}_r = \frac{\mathbf{B}_l}{\cos\alpha}. \quad (1)$$

Here $\mathbf{B}_l$ is the observational line-of-sight magnetic component; $\alpha$ is the angle between line-of-sight direction and normal to the photosphere surface, that depends on heliographic coordinates. Photosphere region, taken as lower boundary, was considered as planar surface and all computations were performed in Cartesian geometry. Computational domains have sizes of ~[240 × 160 × 130] Mm for AR 10314 and ~[180 × 180 × 130] Mm for AR10588.

The potential extrapolation was performed using SOHO/MDI magnetograms, closest by time to the flare events. In order to get exact match by time, minor spatial rotations of the computational domains were made in both cases. The lines of the extrapolated magnetic field are presented in Fig. 8. We used flare X-ray sources to mark position of

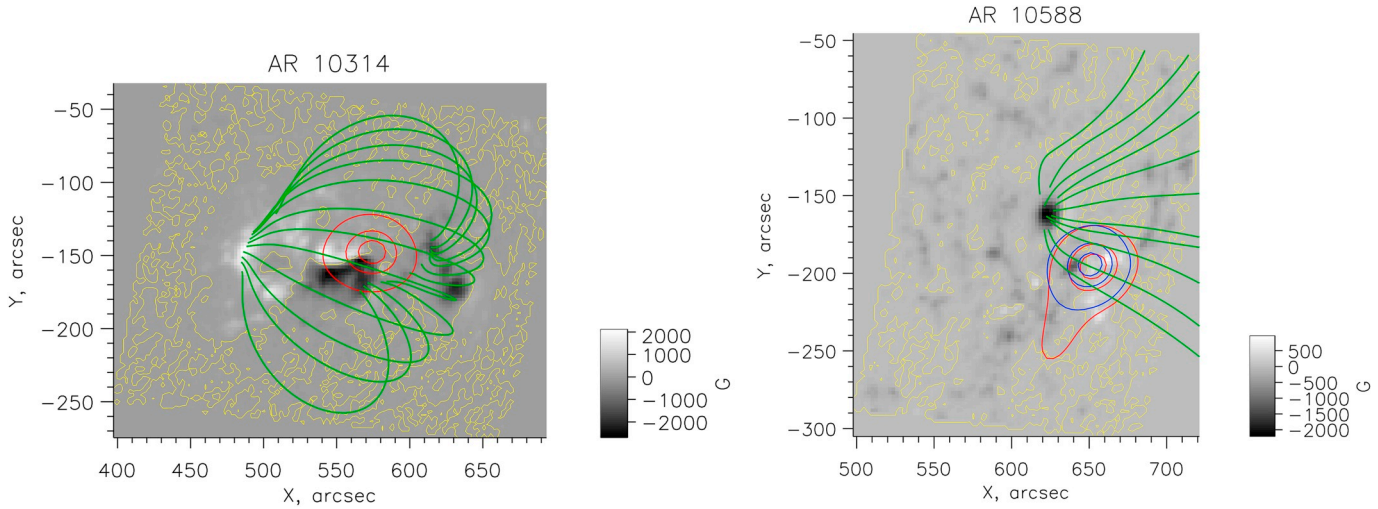


**Fig. 8.** The left panel: The LOS magnetogram by SOHO/MDI of the AR 10314 with the characteristic lines of the extrapolated magnetic field (green color), in projection on the visible solar disk. The white and black background is the radial component of the photosphere magnetic field, the only lower boundary of the computational domain is presented. Yellow contours mark neutral line. The overlaid contours of the X-ray 12 − 25 keV and 25 − 50 keV sources obtained by RHESSI within 04:14:30 − 04:15:30 UT. The contours of X-ray sources are 50, 70 and 90% of the maximum intensity of the X-ray image. The right panel: The same as on the left panel but for AR 10588 and the overlaid contours is the X-ray 12 − 25 keV source only. (For interpretation of the references to color in this figure legend, the reader is referred to the Web version of this article.)

the flare on the LOS magnetograms for both events. Potential extrapolation yields two significantly different configurations of the magnetic field.

In the AR 10314 (Fig. 8, the left panel) high arcade was revealed, that overlaps low lying sigmoid-like structures and reaches height of 70 − 90 Mm while unipolar sunspot of the AR 10588 (Fig. 8, the right panel) had substantial amount of opened magnetic field lines. The magnetic topology of the AR 10314 looks like the topology of the AR 12192 analyzed by Thalmann et al. (2015). The topology of AR 12192 resulted to unusual lack of CME related with the AR in spite of the large amount of the occurred X-class flares. The revealed difference in the large-scale magnetic structure could explain why the C-class event has a greater particle impact on Earth than the X-class flare.

## 3. Discussion and conclusions

We would like to note that the selection of the two flares for the current comparative study seems accidental or fortuitous at first sight. However large statistical studies often analyse for a statistical significance physically different data. We selected the events that are very close by several parameters which are considered during the statistical studies − spectral index of the non-thermal emission of the solar flare, location on the solar disk, CME direction of propagation, electron flux of the SEP event in a selected energy channel. The most interesting contradiction attracting attention is that the weaker event in SXR-emission (C9.6 flare according to GOES classification) turned out to be the origin of a more proton abundant SEP event compared to the more powerful in SXR-emission event (the X1.5 flare). The X-ray photon spectral indexes characterizing the processes of acceleration in solar flares are close to each other within the limits of errors. As it was noted above, the location of the events on the solar disk was very similar and both of them were related with CMEs with the speed above 1000 km $s^{-1}$. The ratio of the CME speed (and AW) of the SOL2004-Apr-11 event to the same parameter of SOL2003-Mar-17 event is 1.6 (whereas it is more then three times wider, respectively) while the lowest factor between the proton fluxes of these events is 17. If we assume that the SEP protons were accelerated or re-accelerated mostly by CME's shock waves, we should expect the more significant difference between the speed of CMEs. The location of both events on the solar disk and direction of propagation were similar. Thus the projection effects could not play a significant role, in this case. It is difficult to explain such difference in the proton fluxes by acceleration on the CME shock wave only.

According to the SXR derivative, the initial phase of SOL2004-Apr-11 flare looks similarly to the initial phase of the M-class flare with γ-ray emission (Ackermann et al., 2012; Kashapova et al., 2012). The electron fluxes indicated by the SXR derivative could be the result of the first stage of acceleration which signatures were too weak to be detected by HXR observations. We speculate that one of the reasons of high levels of SEP protons could be related to this peculiarity in the flare scenario, in spite of the absence of a direct evidence in X-ray and γ-ray emission.

However, we note that during the SOL2004-Apr-11 the first peak at the time profile of the SXR derivative was caused by electrons with energy about 12 − 25 keV and preceded the onset the type III radio bursts that are signatures of electrons going towards the interplanetary space. The duration of this type III was about 10 min. There was a very short burst temporally coinciding with the SXR derivative during the other flare. We can identify this burst as the type III. However, one can note that it occurred after the impulse phase of the SOL2003-Mar-17 event.

The other flare acceleration parameters are very close. However, the maximum intensity of the flux of solar protons with energy above 10 MeV during the SOL2004-Apr-11 event was more than 60 times greater than proton flux during the SOL2003-Mar-17 event. Besides that the spectral properties of SEP proton and electron fluxes are opposite to each other. The SEP proton spectral index in the SOL2004-Apr-11 event was softer than in the SOL2003-Mar-17 event. In contrary, the SEP electron spectral index of the more proton-rich event was harder than in the other event.

Apart from the favourable shock-acceleration for the SOL2004-Apr-11 compared to SOL2003-Mar-17 event, we presume that an additional reason of the observed SEP parameter difference is related to the magnetic topology of the ARs where the events occurred. As it was noted above, the AR 10314 and the SOL2003-Mar-17 flare location were covered by a high arcade reminiscent to the AR considered in Thalmann et al. (2015). We note that in spite of ”closed” magnetic configuration type III bursts were observed during the SOL2003-Mar-17 event. However these type III bursts occurred after the impulsive phase and their duration was very short. A plausible interpretation is that as a result of a magnetic field reconfiguration during the flare, the electrons were allowed to escape the solar atmosphere during a short time. The SOL2003-Mar-17 event was associated with CME but there is no evidence of a filament eruption. Nevertheless, there is information about a failed eruption occurred at 10:42 UT about 8 h before the event onset and CME origin. This appears to be similar to the two-step filament eruption studied by Chandra et al. (2017) where the first step of the process is also associated with a failed filament eruption. There are several groups of models suggesting an explanation and describing processes causing a filament eruption, see, for example, Török et al. (2004) and Török and Kliem (2005) or one of the most recent publications by Kolotkov et al. (2018). Activization of filament could be related to conditions in the surrounding solar atmosphere that result to the zones of the stability or instability at different heights above the filament (see Vršnak, 2008; Kolotkov et al., 2016). The special case of these models is the model consisting of the two critical heights defining the levels of vertical instability initiation of the flux-rope Filippov (2018) We think that it is the most suitable explanation for the current case. The magnetic field in the AR has a two-scale structure and a filament erupts after ascending to the critical height from a metastable level. This model does not assume formation of open magnetic field lines and increasing of the efficiency of the particle escape into interplanetary space.

As it was mentioned above the SOL2004-Apr-11 event occurred in AR 10588. We would like to note that this AR had already attracted interest by the researchers due to the presence of a set of three complex, long-duration, low-frequency type III bursts (Gopalswamy and Mäkelä, 2010). The authors tested if such type III radio burst could be an indicator of SEP events. But they came to the conclusion that only the appearance of such type III radio burst could not be a good indicator of SEP events and all significant SEP events were followed by CMEs, flares and type II bursts. We presume that the location of the origin of the long duration type III radio bursts was closely related with the open magnetic potential lines seen in Fig. 8, right panel.

The existence of open magnetic field lines nearby the energy release location allowed the generated accelerated electrons to effectively escape from the solar atmosphere. It is evident that proton generation in the SOL2004-Apr-11 event could be also associated with CME and the filament eruption. However the magnetic field topology dominated by high open magnetic fields enabled more effective escape of the protons to the IP space that manifested in a relatively soft spectral characteristics of the proton flux. The results of the comparative analysis of these events show that for the occurrence of proton rich SEP events the conditions for particle escape to the IP space are as important as the acceleration processes during the flare. One of the indicators of the existence of advanced possibilities for proton escaping could be the domination of open magnetic field lines in the AR producing the event. However, such peculiarity of the AR magnetic topology is necessary for the production of proton-rich events but not sufficient. Most possibly the flare should also be accompanied by a CME.

This feature could result to high proton fluxes in SEP events compared to events that are also followed by CME but which occurred in an

AR dominated by closed loops. The presented here characteristic of the AR topology as SEP event indicator needs to be verified on a larger data set as a test for statistical significance. Nevertheless, taking into account this parameter could improve or clarify the results of statistical studies.

## Acknowledgements

This study is supported by the project 'The origin on solar energetic particles: solar flares vs. coronal mass ejections', co-funded by the Russian Foundation for Basic Research with project No. 17-52-18050 and the National Science Fund of Bulgaria under contract No. DNTS/Russia 01/6 (23-Jun-2017). Authors are thankful to Sergei Anfinogentov, researcher from Institute of Solar-Terrestrial Physics, for granting his code for potential extrapolation. LK and IM thank the budgetary funding of Basic Research program II.16 and the Program No. 28 of the RAS Presidium for partial support.

## References

Ackermann, M., Ajello, M., Allafort, A., Atwood, W.B., Baldini, L., Barbiellini, G., Bastieri, D., Bechtol, K., Bellazzini, R., Bhat, P.N., Blandford, R.D., Bonamente, E., Borgland, A.W., Bregeon, J., Briggs, M.S., Brigida, M., Bruel, P., Buehler, R., Burgess, J.M., Buson, S., Caliandro, G.A., Cameron, R.A., Casandjian, J.M., Cecchi, C., Charles, E., Chekhtman, A., Chiang, J., Ciprini, S., Claus, R., Cohen-Tanugi, J., Connaughton, V., Conrad, J., Cutini, S., Dennis, B.R., de Palma, F., Dermer, C.D., Digel, S.W., Silva, E.d.C.e., Drell, P.S., Drlica-Wagner, A., Dubois, R., Favuzzi, C., Fegan, S.J., Ferrara, E.C., Fortin, P., Fukazawa, Y., Fusco, P., Gargano, F., Germani, S., Giglietto, N., Giordano, F., Giroletti, M., Glanzman, T., Godfrey, G., Grillo, L., Grove, J.E., Gruber, D., Guiriec, S., Hadasch, D., Hayashida, M., Hays, E., Horan, D., Iafrate, G., Jóhannesson, G., Johnson, A.S., Johnson, W.N., Kamae, T., Kippen, R.M., Knödlseder, J., Kuss, M., Lande, J., Latronico, L., Longo, F., Loparco, F., Lott, B., Lovellette, M.N., Lubrano, P., Mazziotta, M.N., McEnery, J.E., Meegan, C., Mehault, J., Michelson, P.F., Mitthumsiri, W., Monte, C., Monzani, M.E., Morselli, A., Moskalenko, I.V., Murgia, S., Murphy, R., Naumann-Godo, M., Nuss, E., Nymark, T., Ohno, M., Ohsugi, T., Okumura, A., Omodei, N., Orlando, E., Paciesas, W.S., Panetta, J.H., Parent, D., Pesce-Rollins, M., Petrosian, V., Pierbattista, M., Piron, F., Pivato, G., Poon, H., Porter, T.A., Preece, R., Rainò, S., Rando, R., Razzano, M., Razzaque, S., Reimer, A., Reimer, O., Ritz, S., Sbarra, C., Schwartz, R.A., Sgrò, C., Share, G.H., Siskind, E.J., Spinelli, P., Takahashi, H., Tanaka, T., Tanaka, Y., Thayer, J.B., Tibaldo, L., Tinivella, M., Tolbert, A.K., Tosti, G., Troja, E., Uchiyama, Y., Usher, T.L., Vandenbroucke, J., Vasileiou, V., Vianello, G., Vitale, V., von Kienlin, A., Waite, A.P., Wilson-Hodge, C., Wood, D.L., Wood, K.S., Yang, Z., Fermi LAT Collaboration, 2012. Fermi detection of γ-ray emission from the M2 soft x-ray flare on 2010 june 12. Astrophys. J. 745, 144. https://doi.org/10.1088/0004-637X/745/2/144. arXiv:1111.7026.

Akimov, V.V., Ambrož, P., Belov, A.V., Berlicki, A., Chertok, I.M., Karlický, M., Kurt, V.G., Leikov, N.G., Litvinenko, Y.E., Magun, A., Minko-Wasiluk, A., Rompolt, B., Somov, B.V., 1996. Evidence for prolonged acceleration based on a detailed analysis of the long-duration solar gamma-ray flare of June 15, 1991. Sol. Phys. 166, 107–134. https://doi.org/10.1007/BF00179358.

Bazilevskaya, G.A., 2017. Once again about origin of the solar cosmic rays. In: Journal of Physics Conference Series, pp. 012034. https://doi.org/10.1088/1742-6596/798/1/012034.

Bogomolov, A.V., Kashapova, L.K., Myagkova, I.N., Tsap, Y.T., 2014. Dynamics of the hard X-ray, gamma-ray, and microwave emission of solar flares produced by the active region NOAA 0069 in August 2002. Astron. Rep. 58, 156–166. https://doi.org/10.1134/S1063772914030020.

Cane, H.V., Erickson, W.C., Prestage, N.P., 2002. Solar flares, type III radio bursts, coronal mass ejections, and energetic particles. J. Geophys. Res. 107, 1315. https://doi.org/10.1029/2001JA000320.

Cane, H.V., Richardson, I.G., von Rosenvinge, T.T., 2010. A study of solar energetic particle events of 1997-2006: their composition and associations. J. Geophys. Res. 115, A08101. https://doi.org/10.1029/2009JA014848.

Chandra, R., Filippov, B., Joshi, R., Schmieder, B., 2017. Two-step filament eruption during 14 - 15 March 2015. Sol. Phys. 292, 81. https://doi.org/10.1007/s11207-017-1104-5. arXiv:1704.08860.

Chertok, I.M., 1995. Post-eruption particle acceleration in the corona: a possible contribution to solar cosmic rays. International Cosmic Ray Conference 4, 78.

Dennis, B.R., Zarro, D.M., 1993. The Neupert effect - what can it tell us about the impulsive and gradual phases of solar flares? Sol. Phys. 146, 177–190. https://doi.org/10.1007/BF00662178.

Desai, M., Giacalone, J., 2016. Large gradual solar energetic particle events. Living Rev. Sol. Phys. 13, 3. https://doi.org/10.1007/s41116-016-0002-5.

Filippov, B., 2018. Two-step solar filament eruptions. Mon. Not. Roy. Astron. Soc. 475, 1646–1652. https://doi.org/10.1093/mnras/stx3277. arXiv:1712.08173.

Gopalswamy, N., Mäkelä, P., 2010. Long-duration low-frequency type III bursts and solar energetic particle events. Astrophys. J. Lett. 721, L62–L66. https://doi.org/10.1088/2041-8205/721/1/L62.

Gopalswamy, N., Mäkelä, P., Akiyama, S., Yashiro, S., Xie, H., Thakur, N., Kahler, S.W., 2015. Large solar energetic particle events associated with filament eruptions outside of active regions. Astrophys. J. 806, 8. https://doi.org/10.1088/0004-637X/806/1/8. arXiv:1504.00709.

Gopalswamy, N., Yashiro, S., Michalek, G., Stenborg, G., Vourlidas, A., Freeland, S., Howard, R., 2009. The SOHO/LASCO CME catalog. Earth Moon Planets 104, 295–313. https://doi.org/10.1007/s11038-008-9282-7.

Grechnev, V.V., Kurt, V.G., Chertok, I.M., Uralov, A.M., Nakajima, H., Altyntsev, A.T., Belov, A.V., Yushkov, B.Y., Kuznetsov, S.N., Kashapova, L.K., Meshalkina, N.S., Prestage, N.P., 2008. An extreme solar event of 20 january 2005: properties of the flare and the origin of energetic particles. Sol. Phys. 252, 149–177. https://doi.org/10.1007/s11207-008-9245-1. arXiv:0806.4424.

Iucci, N., Levitin, A.E., Belov, A.V., Eroshenko, E.A., Ptitsyna, N.G., Villoresi, G., Chizhenkov, G.V., Dorman, L.I., Gromova, L.I., Parisi, M., Tyasto, M.I., Yanke, V.G., 2005. Space weather conditions and spacecraft anomalies in different orbits. Space Weather 3https://doi.org/10.1029/2003SW000056. s01001. https://doi.org/10.1029/2003SW000056.

Jiggens, P., Chavy-Macdonald, M.A., Santin, G., Menicucci, A., Evans, H., Hilgers, A., 2014. The magnitude and effects of extreme solar particle events. Journal of Space Weather and Space Climate 4, A20. https://doi.org/10.1051/swsc/2014017.

Kahler, S.W., Cliver, E.W., Cane, H.V., McGuire, R.E., Stone, R.G., Sheeley Jr., N.R., 1986. Solar filament eruptions and energetic particle events. Astrophys. J. 302, 504–510. https://doi.org/10.1086/164009.

Kashapova, L.K., Meshalkina, N.S., Kisil, M.S., 2012. Detection of acceleration processes during the initial phase of the 12 june 2010 flare. Sol. Phys. 280, 525–535. https://doi.org/10.1007/s11207-012-0080-z. arXiv:1207.5896.

Klecker, B., Kunow, H., Cane, H.V., Dalla, S., Heber, B., Kecskemety, K., Klein, K.L., Kota, J., Kucharek, H., Lario, D., Lee, M.A., Popecki, M.A., Posner, A., Rodriguez-Pacheco, J., Sanderson, T., Simnett, G.M., Roelof, E.C., 2006. Energetic particle observations. Space Sci. Rev. 123, 217–250. https://doi.org/10.1007/s11214-006-9018-9.

Klein, K.L., Dalla, S., 2017. Acceleration and propagation of solar energetic particles. Space Sci. Rev. 212, 1107–1136. https://doi.org/10.1007/s11214-017-0382-4. arXiv:1705.07274.

Klein, K.L., Trottet, G., 2001. The origin of solar energetic particle events: coronal acceleration versus shock wave acceleration. Space Sci. Rev. 95, 215–225.

Kolotkov, D.Y., Nisticò, G., Nakariakov, V.M., 2016. Transverse oscillations and stability of prominences in a magnetic field dip. Astron. Astrophys. 590, A120. https://doi.org/10.1051/0004-6361/201628501.

Kolotkov, D.Y., Nisticò, G., Rowlands, G., Nakariakov, V.M., 2018. Finite amplitude transverse oscillations of a magnetic rope. J. Atmos. Sol. Terr. Phys. 172, 40–52. https://doi.org/10.1016/j.jastp.2018.03.005. arXiv:1803.05195.

Kuznetsov, S.N., Bogomolov, A.V., Galkin, V.I., Denisov, Y.I., Podorolsky, A.N., Ryumin, S.P., Kudela, K., Rojko, J., 2014. Scientific set of instruments "solar cosmic rays". In: Kuznetsov, V. (Ed.), The Coronas-F Space Mission, pp. 289. https://doi.org/10.1007/978-3-642-39268-9_9.

Kuznetsov, S.N., Kurt, V.G., Myagkova, I.N., Yushkov, B.Y., Kudela, K., 2006. Gamma-ray emission and neutrons from solar flares recorded by the SONG instrument in 2001 2004. Sol. Syst. Res. 40, 104–110. https://doi.org/10.1134/S0038094606020031.

Lin, R.P., Dennis, B.R., Hurford, G.J., Smith, D.M., Zehnder, A., Harvey, P.R., Curtis, D.W., Pankow, D., Turin, P., Bester, M., Csillaghy, A., Lewis, M., Madden, N., van Beek, H.F., Appleby, M., Raudorf, T., McTiernan, J., Ramaty, R., Schmahl, E., Schwartz, R., Krucker, S., Abiad, R., Quinn, T., Berg, P., Hashii, M., Sterling, R., Jackson, R., Pratt, R., Campbell, R.D., Malone, D., Landis, D., Barrington-Leigh, C.P., Slassi-Sennou, S., Cork, C., Clark, D., Amato, D., Orwig, L., Boyle, R., Banks, I.S., Shirey, K., Tolbert, A.K., Zarro, D., Snow, F., Thomsen, K., Henneck, R., McHedlishvili, A., Ming, P., Fivian, M., Jordan, J., Wanner, R., Crubb, J., Preble, J., Matranga, M., Benz, A., Hudson, H., Canfield, R.C., Holman, G.D., Crannell, C., Kosugi, T., Emslie, A.G., Vilmer, N., Brown, J.C., Johns-Krull, C., Aschwanden, M., Metcalf, T., Conway, A., 2002. The reuven ramaty high-energy solar spectroscopic imager (RHESSI). Sol. Phys. 210, 3–32. https://doi.org/10.1023/A:1022428818870.

Miteva, R., Samwel, S.W., Costa-Duarte, M.V., 2018. The wind/EPACT proton event catalog (1996 - 2016). id. 27. Sol. Phys. 293https://doi.org/10.1007/s11207-018-1241-5. arXiv:1801.00469.

Moses, D., Clette, F., Delaboudinière, J.P., Artzner, G.E., Bougnet, M., Brunaud, J., Carabetian, C., Gabriel, A.H., Hochedez, J.F., Millier, F., Song, X.Y., Au, B., Dere, K.P., Howard, R.A., Kreplin, R., Michels, D.J., Defise, J.M., Jamar, C., Rochus, P., Chauvineau, J.P., Marioge, J.P., Catura, R.C., Lemen, J.R., Shing, L., Stern, R.A., Gurman, J.B., Neupert, W.M., Newmark, J., Thompson, B., Maucherat, A., Portier-Fozzani, F., Berghmans, D., Cugnon, P., van Dessel, E.L., Gabryl, J.R., 1997. EIT observations of the extreme ultraviolet Sun. Sol. Phys. 175, 571–599. https://doi.org/10.1023/A:1004902913117.

Neupert, W.M., 1968. Comparison of solar x-ray line emission with microwave emission during flares. Astrophys. J. Lett. 153, L59. https://doi.org/10.1086/180220.

Núñez, M., 2011. Predicting solar energetic proton events (E > 10 MeV). Space Weather 9, 07003. https://doi.org/10.1029/2010SW000640.

Scherrer, P.H., Bogart, R.S., Bush, R.I., Hoeksema, J.T., Kosovichev, A.G., Schou, J., Rosenberg, W., Springer, L., Tarbell, T.D., Title, A., Wolfson, C.J., Zayer, I., MDI Engineering Team, 1995. The solar oscillations investigation - Michelson Doppler imager. Sol. Phys. 162, 129–188. https://doi.org/10.1007/BF00733429.

Schwartz, R.A., Csillaghy, A., Tolbert, A.K., Hurford, G.J., McTiernan, J., Zarro, D., 2002. RHESSI data analysis software: rationale and methods. Sol. Phys. 210, 165–191. https://doi.org/10.1023/A:1022444531435.

Semkova, J., Koleva, R., Benghin, V., Dachev, T., Matviichuk, Y., Tomov, B., Krastev, K., Maltchev, S., Dimitrov, P., Mitrofanov, I., Malahov, A., Golovin, D., Mokrousov, M., Sanin, A., Litvak, M., Kozyrev, A., Tretyakov, V., Nikiforov, S., Vostrukhin, A., Fedosov, F., Grebennikova, N., Zelenyi, L., Shurshakov, V., Drobishev, S., 2018. Charged particles radiation measurements with Liulin-MO dosimeter of FREND instrument aboard ExoMars Trace Gas Orbiter during the transit and in high elliptic Mars orbit. Icarus 303, 53–66. https://doi.org/10.1016/j.icarus.2017.12.034.

Stone, E.C., Frandsen, A.M., Mewaldt, R.A., Christian, E.R., Margolies, D., Ormes, J.F., Snow, F., 1998. The advanced composition explorer. Space Sci. Rev. 86, 1–22. https://doi.org/10.1023/A:1005082526237.

Thalmann, J.K., Su, Y., Temmer, M., Veronig, A.M., 2015. The confined x-class flares of solar active region 2192. Astrophys. J. Lett. 801, L23. https://doi.org/10.1088/2041-8205/801/2/L23. arXiv:1502.05157.

Török, T., Kliem, B., 2005. Confined and ejective eruptions of kink-unstable flux ropes. Astrophys. J. Lett. 630, L97–L100. https://doi.org/10.1086/462412. arXiv:astro-ph/0507662.

Török, T., Kliem, B., Titov, V.S., 2004. Ideal kink instability of a magnetic loop equilibrium. Astron. Astrophys. 413, L27–L30. https://doi.org/10.1051/0004-6361:20031691. arXiv:astro-ph/0311198.

Torsti, J., Valtonen, E., Lumme, M., Peltonen, P., Eronen, T., Louhola, M., Riihonen, E., Schultz, G., Teittinen, M., Ahola, K., Holmlund, C., Kelhä, V., Leppälä, K., Ruuska, P., Strömmer, E., 1995. Energetic particle experiment ERNE. Sol. Phys. 162, 505–531. https://doi.org/10.1007/BF00733438.

Vainio, R., Afanasief, A., 2018. Particle Acceleration Mechanisms. Solar Particle Radiation Storms Forecasting and Analysis, Astrophysics and Space Science Library, vol 444. Spinger, Cham, pp. 45–61. https://doi.org/10.1007/978-3-319-60051-2_3.

Vršnak, B., 2008. Processes and mechanisms governing the initiation and propagation of CMEs. Ann. Geophys. 26, 3089–3101. https://doi.org/10.5194/angeo-26-3089-2008.

Wang, Y.M., Sheeley Jr., N.R., 1992. On potential field models of the solar corona. Astrophys. J. 392, 310–319. https://doi.org/10.1086/171430.

Zhao, X., Liu, Y.D., Inhester, B., Feng, X., Wiegelmann, T., Lu, L., 2016. Comparison of CME/Shock propagation models with heliospheric imaging and in situ observations. Astrophys. J. 830, 48. https://doi.org/10.3847/0004-637X/830/1/48. arXiv:1607.05533.

Zimovets, I., Struminsky, A., 2012. Non-thermal “Burst-on-Tail” of long-duration solar event on 26 october 2003. Sol. Phys. 281, 749–763. https://doi.org/10.1007/s11207-012-0112-8. arXiv:1205.3719.